Designing photonic structures of nanosphere arrays on reflectors for total absorption

E. Almpanis and N. Papanikolaou

Citation: Journal of Applied Physics **114**, 083106 (2013); doi: 10.1063/1.4818916
View online: http://dx.doi.org/10.1063/1.4818916
View Table of Contents: http://scitation.aip.org/content/aip/journal/jap/114/8?ver=pdfcov
Published by the AIP Publishing

JOURNAL OF APPLIED PHYSICS **114**, 083106 (2013)

Designing photonic structures of nanosphere arrays on reflectors for total absorption

E. Almpanis and N. Papanikolaou
Department of Microelectronics, IAMPPNM, NCSR "Demokritos," GR-153 10 Athens, Greece

(Received 22 April 2013; accepted 5 August 2013; published online 23 August 2013)

By means of full electrodynamic simulations, we investigate structures that can totally absorb light minimizing all reflections. Such efficient absorbers of visible and infrared light are useful in photovoltaic and sensor applications. Our study provides a simple and transparent analysis of the optical properties of structures comprising a resonant cavity and a reflector, which are the basic ingredients of a resonant absorber, based on general principles of scattering theory. We concentrate on periodic arrays of metallic or dielectric spherical particles in front of metallic or dielectric mirrors and show that tuning the material absorption could turn resonances in the structures into total absorption bands. Perfect absorption is predicted in metallic sphere arrays but also for Si spheres on a metallic substrate, moreover, by replacing the substrate below the Si spheres with a lossless dielectric Bragg mirror an all-dielectric-perfect-absorber is designed. © *2013 AIP Publishing LLC*.
[http://dx.doi.org/10.1063/1.4818916]

I. INTRODUCTION

The development of smart surfaces that absorb electromagnetic (EM) waves has been driven by microwave and radar technology many years ago. Matching the impedance to the environment of the incident radiation, using interfaces with a graded index of refraction, is one way to reduce scattering losses. Alternatively, different reflective layers can be used to achieve destructive interference, and thus, reduce the scattered radiation. Two of the oldest and simplest types of absorbers are the Salisbury screens and the Dallenbach layers.[1] The Salisbury screen is a resonant absorber created by placing a resistive sheet on a low-dielectric-constant spacer in front of a metal plate. The Dallenbach layer consists of a homogeneous lossy layer on top of a metallic plate. Recently, there is renewed interest on surfaces that strongly absorb visible and near-infrared light. Current interest is mainly driven by energy harvesting and optical sensors applications and aims at steering light in optically active regions in a device as well as focusing in subwavelength dimensions. Given the optical properties of the technologically available materials, current micro and nanofabrication tools provide extra degrees of freedom for engineering absorption at these wavelengths by patterning the surface in the micro/nanoscale. In particular, thin discontinuous metal films[2] and nanostructured metallic surfaces exhibit a variety of intriguing optical properties and allow for a variety of resonant absorbers designs. Subwavelength structures based on metal-insulator-metal (MIM) involving Fabry-Perot-like resonances are also often used to obtain enhanced absorption. Moreover, carefully designed metamaterial-based total absorbers, which localize light strongly, were also studied.[3–21] Such effects are usually related to plasmonic excitations and are very promising in the way of practical applications in photovoltaic cells,[22–25] visible and infrared sensors,[3,26] and detectors.[27]

The scattering properties of single plasmonic nanoparticles have also drawn some attention recently. In particular, metal-dielectric-metal meta-atoms with enhanced scattering have been theoretically analyzed[28] and systematic studies of the absorption properties of spherical nanoparticles of different metals have been reported.[29,30]

By generalizing the concept of critical coupling to a nanocavity with surface plasmon resonances, it was predicted[31] that coherent light can be completely absorbed and transferred to surface plasmons in a metallic nanostructure. The concept is general and can be understood as a time-reversed process of the corresponding surface plasmon laser. However, the creation of coherent light might be a constraint for complex metallodielectric nanostructures. On the other hand, the same principles are applicable to absorber designs with resonators in front of a mirror. The presence of a reflector is useful since, by carefully designing the resonator, total absorption condition could be possible for plane wave incident radiation. In the present work, we shall be concerned with such perfect absorbers, consisting of periodic arrays of micro and nanoparticles on top of a reflector.

Resonant absorbers have a limited spectral range. The plasmon-based total absorbers show reduced linewidths, which are beneficial for sensing applications based on refractive index change. Introducing structures that support multiple resonances can increase the width of the absorption band,[3,6,7,18,32] which is useful in photovoltaics and thermophotovoltaics, but also in an attempt to replace traditional absorbers with subwavelength thin metamaterial absorbers for microwaves.[19] Moreover, non-resonant, broadband absorption using ultra-sharp convex metal grooves via adiabatic nanofocusing of gap surface plasmon modes excited by scattering off subwavelength-sized wedges was reported,[33] while widening of the absorption spectra by combining two MIM ribbons with different widths in the same subwavelength period was also considered.[18]

A basic ingredient in many of the attempts to design perfect absorbers is the presence of a metallic material. Its role is twofold: It localizes the EM energy in small subwavelength volumes and at the same time the excited electrons of the metal are responsible for absorbing light through Joule effect. Recently, some attempts with dielectric absorbers have also been reported.[34,35] Moreover, total absorption in an optically dense planar grid of plasmonic nanoparticles over a transparent, high-index, dielectric substrate was also investigated.[36] One of the most successful and, due to its simplicity, widely used designs is a periodic array of metallic nanoparticles or stripes in close proximity to an optically thick metallic film. The absorption band can be easily tuned within the visible and infrared part of the spectrum by varying the dimensions of the structure. Symmetric nanoparticle arrays are polarization insensitive, while for metallic stripes or particles that brake the in-plane (x-y) symmetry absorption strongly depends on polarization, which provides more design options, depending on the application. Moreover, in many cases, absorption shows small dispersion with the incidence angle, resulting in broad-angle absorbers.[6,13,15,17,18]

The condition for perfect absorption corresponds to the zeros of the determinant of the scattering S matrix, which connects the incoming to the outgoing field after scattering, i.e., formally $|\text{out}>=S|\text{in}>$. For a lossless structure, the perfect absorption condition to have a vanishing outgoing field leads to the trivial solution $|\text{in}>=0$, since the condition $detS=0$ is satisfied only for complex frequencies. However, if losses are introduced, it is possible that some of the zeros of the eigenvalues of the S matrix move to the real axis and the perfect absorption condition is satisfied.[37] This is often called critical coupling condition,[38] at which the internal, non-radiative loss rate γ_{nr} matches the radiation scattering rate γ_{rad}. The imaginary part of the dielectric function (Imε), which determines material absorption, together with the modal shape of the resonance are both critical parameters and can be tailored to achieve total absorption using metals or dielectrics.

Recent studies elaborated on the general case of a multiport resonator and derived the critical coupling condition $\gamma_{rad}=\gamma_{nr}$ in a general way.[38] The concept was also demonstrated theoretically for isolated metallic spheres and cylinders,[31] but in the latter case, the required input field must be monochromatic and coherent. For spherical or cylindrical structures, this means converging spherical or cylindrical transverse magnetic (TM) waves, which can be hard to realize experimentally.

In the present work we consider light absorption from surfaces decorated with periodic arrays of spherical particles in front of a reflector. The presence of a reflector offers a wideband background for destructive interference, and we consider an incoming plane wave for frequencies below the first diffraction edge. High, and in most cases total, absorption is predicted for metallic or dielectric particles in front of a metallic film or a dielectric Bragg mirror. After a short description of our computational methodology, we first use a generalized Drude model to describe a metallic nanoparticle array in front of a metallic film and illustrate our analysis. Then we demonstrate that almost total absorption can be obtained with metals and dielectrics, described by experimentally fitted optical constants, and present four different geometries: (i) Ag spheres on a Ag film, (ii) Ag spheres on a dielectric Bragg mirror, (iii) silicon spheres on a Ag film, and (iv) an all dielectric structure with spheres on a Bragg mirror. A theoretical analysis of the critical coupling effect and the connection of the absorption and the local density of states (LDOS) on the radiative and non radiative decay rates is presented in the appendix.

II. COMPUTATIONAL METHOD

We use the layer-multiple-scattering (LMS) method to study the optical properties of highly absorbing, periodically patterned surfaces. The LMS method is a very powerful computational tool for studying three dimensional (3D) photonic crystals consisting of non-overlapping spherical particles (scatterers) in a homogeneous host medium.[39,40] The method can directly provide the transmission, reflection, and absorption coefficients of an incoming EM wave of any polarization incident at a given angle on a finite slab of the crystal and, therefore, it can describe an actual transmission experiment. A further advantage of the method is that it does not require periodicity in the direction perpendicular to the layers, which must only have the same 2D periodicity. The properties of the individual scatterers enter through the corresponding scattering T matrix which, for homogeneous spherical particles, is given by the closed-form solutions of the Mie-scattering problem. At a first step, in-plane multiple scattering is evaluated in a spherical-wave basis using proper propagator functions, where angular momentum expansion up to $\ell_{max}=18$ is sufficient to obtain convergence, for the structures considered here. Subsequently, interlayer scattering is calculated in a plane-wave basis through appropriate reflection and transmission matrices, where 81 plane waves are typically used in the expansion. The scattering S matrix of a multilayer slab, which transforms the incident into the outgoing wave field, is obtained by combining the reflection and transmission matrices of the individual component layers in an appropriate manner. As a special case, a layer can be a homogeneous plate or a planar interface between two different homogeneous media. The reflection and transmission matrices are then obtained directly by Fresnel equations and this possibility allows one to describe composite structures which are used in an actual experiment and include, e.g., a homogeneous spacer layer and/or a supporting substrate. The ratio of the transmitted or reflected energy flux to the energy flux associated with the incident wave defines the transmittance, $\mathcal{T}$, or reflectance, $\mathcal{R}$, of the slab, while absorbance, $\mathcal{A}$, is obtained through $\mathcal{A}=1-\mathcal{R}-\mathcal{T}$.

III. RESULTS AND DISCUSSION

A. Metallic spheres on top of a metallic film

We start our discussion by considering an array of metallic spheres of radius $R=70\,\text{nm}$ arranged on a square lattice with lattice constant $a=160\,\text{nm}$ on top of an 100 nm, optically thick, metallic film, separated by a 10 nm thick SiO_2 layer, in air, as shown in Fig. 1(a). Before presenting

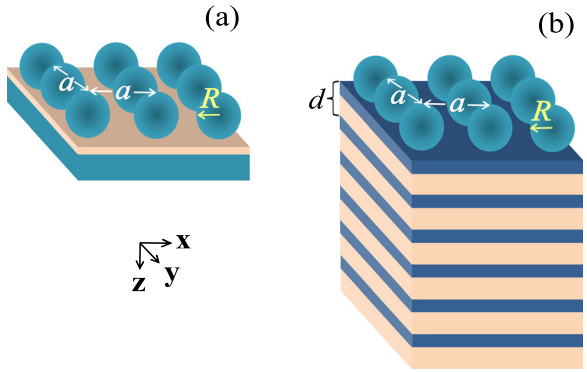

FIG. 1. Schematic of the structures considered in this work. (a) Periodic array of spheres on a metallic substrate with a thin dielectric spacer. (b) Periodic array of spheres on top of a multilayer Bragg mirror.

the results obtained with the realistic optical constants for Ag, we use a modified Drude model to describe the metal dielectric function

$$\epsilon_{met} = \epsilon_\infty - \frac{\omega_P^2}{\omega^2 + i\omega\tau^{-1}}. \quad (1)$$

This function with $\epsilon_\infty = 3.718$, $\hbar\omega_P = 9.176\,\text{eV}$, $\hbar\tau^{-1} = 0.021\,\text{eV}$ can describe satisfactorily the optical response of Ag in the visible, below 3 eV. The SiO_2 dielectric function was assumed constant: $\varepsilon_{SiO_2} = 2.13$. This model is useful since it allows the investigation of the influence of material losses on the optical response in a systematic manner.

For normally incident light, the structure is highly reflective but has absorption resonances at the frequencies of plasmon excitations. Structures with thinner metallic layers have been also studied previously and show enhanced, extraordinary, optical transmission.[41] We focus our attention on a particular mode around 2.96 eV. This mode derives from a delocalized plasmon mode of the film and is characterized by strong absorption and strong field enhancement in the region where the spheres approach the metal film. The frequency of the mode is sensitive to small changes in the thickness of the SiO_2 spacer. In Fig. 2(a), we show the change of the absorption spectra for different values of the inverse Drude relaxation time τ^{-1}, appearing in Eq. (1). As shown in the appendix, the absorption has a Lorentzian form with the half width at half maximum (HWHM) being equal to the total decay rate $\gamma_{tot} = \gamma_{rad} + \gamma_{nr}$. For the Drude dielectric function of Eq. (1), absorption reaches values close to 60%. By increasing τ^{-1} by 4.6 times, we reach perfect, 100%, absorption, but further increase reduces the peak maximum. The absorption is accompanied by a strong field concentration in the region between the sphere and the film as shown in Fig. 2(b). The radiative decay rate, γ_{rad}, does not depend on the absorption and can be extracted from the photonic LDOS by fitting to Eq. (A2). This is calculated by neglecting absorptive losses ($\tau^{-1} = 0$) and is shown in Fig. 3(a). By progressively increasing τ^{-1}, we increase γ_{nr}, and it is possible to determine γ_{tot} from the HWHM of the corresponding absorption spectra. This is shown in Fig. 3(b) together with the variation of the absorption maximum. It is worth to point out that γ_{tot} determined from the absorption spectra,

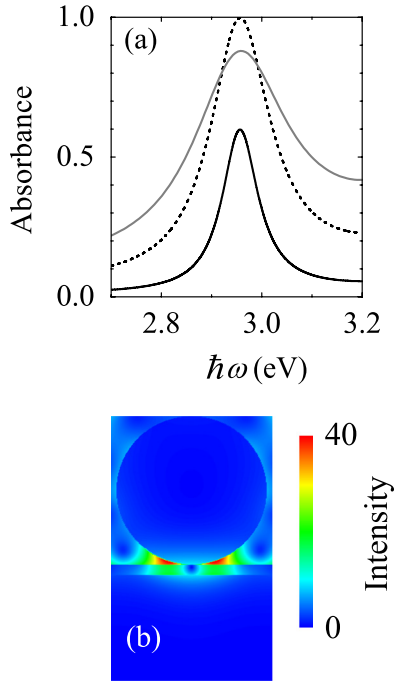

FIG. 2. (a) Absorption spectra of light incident normally on a square array, ($a = 160\,\text{nm}$), of metallic spheres of radius 70 nm on top of a metallic film, of thickness 100 nm separated by a 10 nm thick SiO_2 layer as depicted in Fig. 1(a). The calculations are carried out using the modified Drude dielectric function of Eq. (1) (black line), and inverse relaxation time increased by a factor of 4.6 (dashed line) and 10 (gray line). (b) Profile of the electric field intensity, normalized to that of the incoming field, for the system with maximum peak absorption (dashed line of (a)) at the frequency of total absorption.

extrapolated to $\tau^{-1} = 0$, matches exactly γ_{rad} determined from LDOS. The critical coupling condition is satisfied exactly and absorption reaches the maximum 100% when $\gamma_{tot} = 2\gamma_{rad}$. For stronger losses, γ_{tot} does not vary linearly with τ^{-1}, and also the fit of the absorption to a Lorentzian is more difficult since the peaks are too broad and overlap between neighboring resonances is strong. Alternatively, using Eq. (A4) to fit the absorption spectrum, it is possible to extract the total, the radiative, and the non-radiative decay rates, from a single spectrum. The latter method is also reliable and reproduces the values extracted with the previous procedures. The same approach can be used on experimental spectra.

As already noted before,[37] an arbitrary body or aggregate can be made perfectly absorbing at discrete frequencies if a precise amount of dissipation is added under specific conditions of coherent monochromatic illumination. Assuming linear dependence of γ_{tot} on the absorption controlled by τ^{-1}, if the slope is known, we can predict the amount of loss that is required to achieve perfect absorption. Therefore, LDOS of the lossless structure can be used as a guide for the design of efficient absorbers. Generally, structures that support sharp resonances, when losses are ignored, are expected to become perfect absorbers if some low loss comes into play. On the other hand, broader resonances require materials with large imaginary part of the dielectric function to yield perfect absorption.

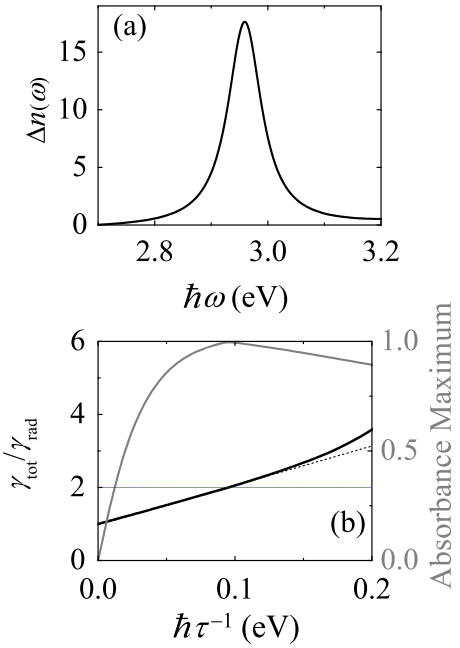

FIG. 3. (a) Change of the density of photonic states for the structure of Fig. 1(a) with the same parameters as in Fig. 2 but using the modified Drude dielectric function of Eq. (1) with $\tau^{-1} = 0$. (b) Black line (left scale): ratio of $\gamma_{tot}/\gamma_{rad}$ extracted by fitting the absorption spectra to Eq. (A4) versus the inverse Drude relaxation time, and the dotted line is a linear interpolation. The horizontal line marks the critical coupling condition. Gray line (right scale): Maximum value of the corresponding absorption peak.

Perfect absorbers can be designed using periodic particle arrays, since by varying the geometry, it is possible to fulfill the critical coupling condition for a given material absorption. To demonstrate this, we have chosen four different examples using realistic optical constants of metals and dielectrics and present structures where absorption is maximized.

In Fig. 4, we present the absorption spectra calculated with the realistic optical parameters of Ag interpolated from the tabulated data of Johnson and Christy,[42] that will be used from now on to describe Ag, for a structure shown in Fig. 1(a) with spheres of $R = 65$ nm, lattice constant $a = 150$ nm, and a 3 nm thick SiO_2 spacer layer on a 100 nm thick Ag film. At normal incidence, total absorption is predicted close to 2.68 eV while a somewhat smaller value is expected around 3.18 eV. The lower frequency mode has a field profile similar to the one shown in Fig. 2(b) with strong field concentration between the sphere and the metallic film. What is interesting however is the angular dispersion of the modes. In Figs. 4(b) and 4(c), we present the absorption for TM and transverse electric (TE) polarized light incident at an angle in the x-z plane. The higher frequency mode has a flat dispersion only for TE polarized light and shows a splitting for TM polarization. The low frequency mode on the other hand has almost flat dispersion with absorption close to one, even at large angles of incidence, up to the light line, for both polarizations, i.e., this mode induces efficient broad-angle absorption. Modes with similar characteristics to the latter one are reported in realizations of efficient absorbers involving particle arrays and a metallic film, and have been exploited to achieve improved photovoltaic designs,[24] and sensitive sensors in visible and infrared frequencies.[26]

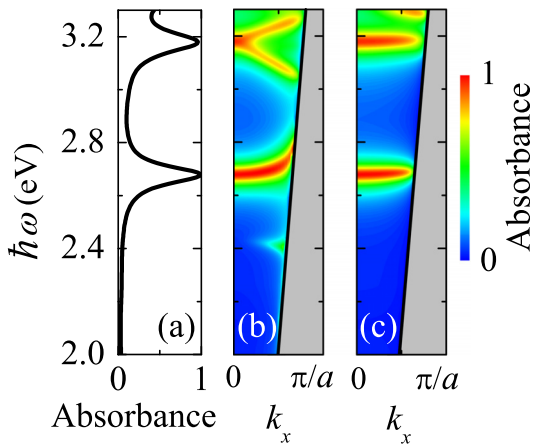

FIG. 4. (a) Absorption spectra of light incident normally on a square array of lattice constant 150 nm of Ag spheres of radius 65 nm on top of a Ag film, of thickness 100 nm separated by a 3 nm thick SiO_2 spacer. Absorption spectra for (b) TM and (c) TE polarized light incident at an angle in the xz-plane versus the corresponding x component of the wave vector. The straight lines mark the light line in air.

B. Silver spheres on a Bragg mirror

The metallic components are not essential to achieve total absorption. For example, the metallic layer below the metallic spheres acts mainly as a reflector and can be replaced by a lossless dielectric Bragg mirror. To demonstrate this, we have calculated the optical response of an array of silver spheres on top of a TiO_2/SiO_2 Bragg mirror which exhibits a band gap in the frequency region under consideration. Similar to the previous structure, we consider an array of Ag spheres with radius $R = 65$ nm arranged in a square lattice with $a = 150$ nm on top of six periods of alternated TiO_2(45 nm)/SiO_2(65 nm) layers, schematically shown in Fig. 1(b), with $\varepsilon_{TiO_2} = 6.25, \varepsilon_{SiO_2} = 2.13$. As shown in Fig. 5(a), as the number of periods of the Bragg mirror increases, and so does the reflectivity, the plasmonic resonance of the metallic spheres at 3.15 eV is turned into a total absorption band, while strong absorption also occurs around 3.4 eV. The electric field profile associated with the total absorption resonance is very similar to the previous case of the metallic mirror showing strong field localization in the region where the spheres touch the flat surface. In this system, absorption takes place in the metallic spheres only, since the dielectrics are assumed to be lossless, but the analysis with the decay rates evaluated from the appropriate resonance widths still holds and leads to similar conclusions. The role of the mirror here is limited to the creation of the strongly localized resonant mode as a result of the interaction with the plasmon resonance of the metallic spheres. The dispersion of the absorbing modes is shown in Figs. 5(b) and 5(c). For the lower frequency resonance, the dielectric mirror causes a shift of the absorption band for TM polarization, pushing the resonance to higher frequencies with increasing angle of incidence. For TE polarization, the absorption band is not shifted, but at large angles of incidence, as we approach the light line, we observe the interaction with the slab modes of the dielectric mirror. The higher frequency

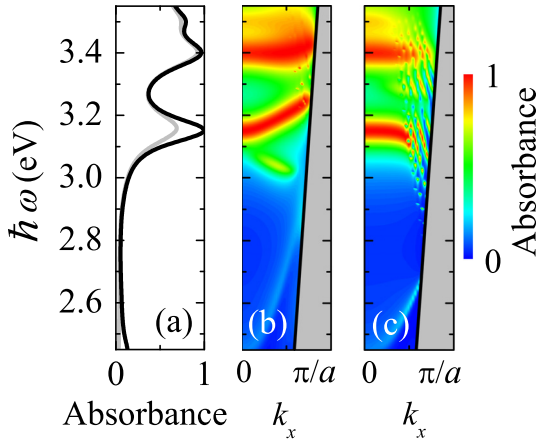

FIG. 5. (a) The same as in Fig. 4 but with the Ag film and SiO_2 spacer replaced by a dielectric Bragg mirror consisting of six periods of alternated TiO_2(45 nm)/SiO_2(65 nm) layers. The gray line in (a) refers to the array of spheres deposited on top of 45 nm thick TiO_2 film on a semi-infinite SiO_2 substrate. Absorption spectra for (b) TM and (c) TE polarized light incident at an angle in the xz-plane versus the corresponding x component of the wave vector. The straight lines mark the light line in air.

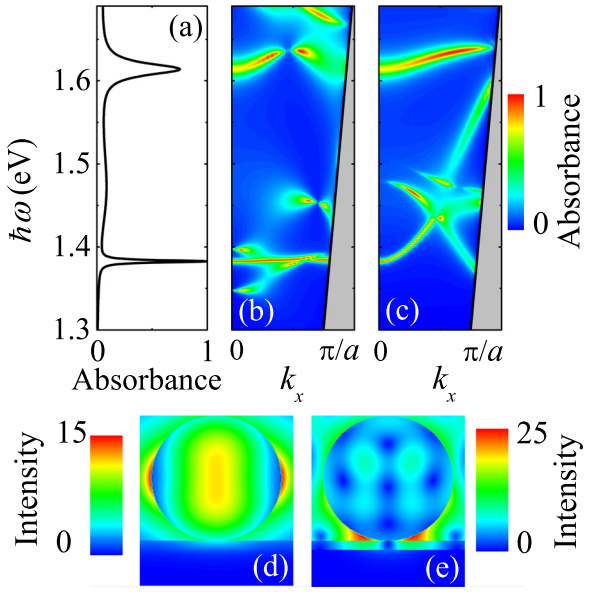

FIG. 6. (a) Absorption spectra of light incident normally on a square array, of lattice constant 360 nm, of Si spheres, of radius 170 nm, on top of a 100 nm thick Ag film separated by a 25 nm thick SiO_2 spacer, in air (see Fig. 1(b)). Absorption for TM (b) and TE (c) polarized light incident at an angle in the x-z plane versus the corresponding x-component of the wavevector. The strong lines mark the light line in air. (d) Electric field intensity profile, normalized to that of the incoming field, associated with the low (d) and the high (e) frequency resonances of Fig. 6(a).

resonance for TM polarization shows no dispersion, while for TE polarization, there is a stronger signature of the Bragg mirror slab modes.

Comparing these results with the case of Ag spheres on a Ag film, we see that total absorption at normal incidence is possible in both systems; however, the metallic film gives a mode with flat dispersion, which is useful in applications where broad-angle absorption is important.

C. Dielectric spheres on top of a metallic film

The spherical particles considered in the previous two examples act as resonators, and metals could be replaced by lossy dielectrics. To elucidate that, we consider a periodic array of Si spheres on top of a 100 nm, optically thick, Ag film separated by a 25 nm thick SiO_2 spacer. The spheres have a radius of 170 nm and are arranged on a square lattice with lattice constant 360 nm. The absorption spectrum of this system, using realistic optical constants for both silver[42] and silicon,[43] is shown in Fig. 6(a). In the frequency range considered, just above the silicon electronic band gap, absorption is moderate, and we find two absorption peaks. The lower frequency resonance is sharper, giving rise to almost total absorption (99.7%) and it corresponds to a strong field localization in the region between the spheres. The other resonance appears at higher frequency, it is broader, and the associated field distribution is mostly localized in the region where the spheres touch the substrate. This modal shape is similar to that of the corresponding mode discussed previously in relation to the metallic spheres. The occurrence of a frequency where perfect absorption takes place depends on the interplay between material absorption and quality factor of the resonance. Replacing metallic spheres with dielectric ones results in sharper resonances and offers the possibility to realize strong absorption with weakly absorbing materials. It is to be noted that, despite the fact that larger radii are required to support (Mie) resonances in dielectrics, as compared to metals, the EM field can be strongly localized in subwavelength volumes, as seen in the field profiles in Fig. 6. It is also interesting that losses occur mainly in silicon. Our calculations show that ignoring the losses in silicon by setting $\mathrm{Im}\varepsilon_{\mathrm{Si}} = 0$ lowers the maximum absorption of the resonance at 1.38 eV to 8% and of the second resonance (at 1.61 eV) to 12%. We obtained similar results for low-refractive-index dielectric spheres, e.g., made of silica or of a polymer material, on a metallic substrate. Experimental studies of such structures with polystyrene[44] and silica[45] spheres on a metallic film were recently reported and show multiple sharp absorption peaks depending on the geometry. However, due to the low losses of silica and polymers at visible and near infrared frequencies, we obtain absorption lower than 85%, for realistic material parameters. The angle dependence of the absorption is shown in Figs. 6(b) and 6(c). For metallic particles above a metal film, discussed previously, absorption is related to plasmon excitation which has a flat dispersion. For Si spheres, absorption of the low frequency mode for TM polarized light persists with only a small frequency shift, up to large angles of incidence, while for TE polarized light, the absorption band shows strong dispersion, with the maximum dropping down and moving to higher frequencies with increasing angle of incidence. The behavior of the high frequency mode is more complex and shows strong dispersion for both polarizations.

D. All-dielectric perfect absorbers

Following the previous analysis, metals can be avoided and sharp resonances can lead to perfect absorption with low loss materials, so as a final example, we consider high-refractive-index dielectric spheres with $\mathrm{Re}\varepsilon_{\mathrm{sph}} = 12$ on a

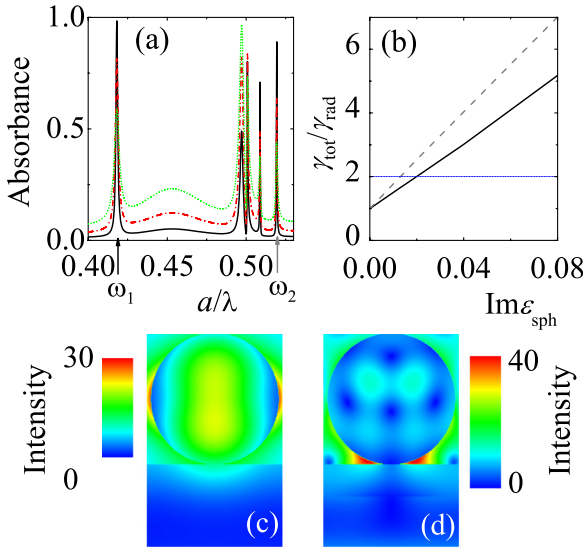

FIG. 7. (a) Absorption spectra of light incident normally on a square array of dielectric spheres on top of a TiO_2/SiO_2 Bragg mirror for different values of the dielectric constant of the spheres. $\varepsilon_{sph} = 12 + i0.02$: black full line, $\varepsilon_{sph} = 12 + i0.05$: red dashed line, $\varepsilon_{sph} = 12 + i0.10$: green dashed-dotted line. (b) Ratio of the total to the radiative decay rates for two of the resonances shown in (a), ω_1: full line, ω_2: dashed line. The horizontal line marks the critical coupling condition. (c) Electric field profile, normalized to that of the incoming field, for spheres with $\varepsilon_{sph} = 12 + i0.02$ at ω_1. (d) Field profile for spheres with $\varepsilon_{sph} = 12 + i0.02$ at ω_2.

lossless Bragg mirror. Using dispersionless optical constants allows us to present the results in scaled units. In Fig. 7, we show the absorption spectra for different values of $\mathrm{Im}\varepsilon_{sph}$ for a periodic array of dielectric spheres of radius $R = 0.8d$, where d is the multilayer periodicity (see Fig. 1), arranged on a square lattice with $a = 1.7d$ on top of a Bragg mirror, consisting of 6 periods of $TiO_2(0.4d)/SiO_2(0.6d)$ layers. The spectrum is characterized by a series of sharp absorption peaks, with their maxima strongly depending on the imaginary part of the dielectric constant. We focus on two characteristic resonance peaks. The first one close to $\omega_1 = 0.42a/\lambda$ gives almost total absorption (99%) for moderate $\mathrm{Im}\varepsilon_{sph}(= 0.02)$. The associated field intensity pattern shows strong enhancement in the region where the spheres approach each other in the lattice. The second resonance, at $\omega_2 = 0.52a/\lambda$, corresponds to the strongest field, which is mainly concentrated in the region where the spheres touch the upper TiO_2 layer of the Bragg mirror. A mode with similar field profile is found in all configurations we studied previously and is expected to give a strongly absorbing band. In Fig. 7(b), we plot the variation of $\gamma_{tot}/\gamma_{rad}$ for the two absorption resonances, at ω_1 and ω_2, versus $\mathrm{Im}\varepsilon_{sph}$. We observe a linear increase with a different slope for each resonance, which depends on the modal shape as well as on the absorption of the different materials in the structure. In any case, it is possible to predict the exact amount of losses required to reach the critical coupling condition and achieve perfect absorption. Such calculations can help the design of total absorbers if the dielectric material losses can be tailored, for example, by chemical modification, controlling the surface roughness, or even by inserting a thin highly absorptive layer in the regions of high field concentration.

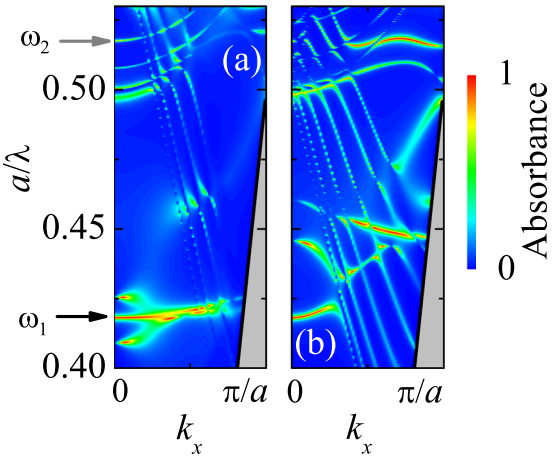

FIG. 8. Absorption spectra for a square array of dielectric spheres ($\varepsilon_{sph} = 12 + i0.02$) on top of a lossless TiO_2/SiO_2 Bragg mirror for (a) TM and (b) TE polarized light incident at an angle in the xz-plane versus the corresponding x component of the wave vector. The straight lines mark the light line in air.

Another interesting aspect of this structure is the angular dispersion of the absorption. This is shown in Fig. 8. There are many similarities of these spectra to those obtained for the array of Si spheres on top of the Ag mirror (see Fig. 6). The low frequency resonance ω_1 shows only a weak angle dependence for the TM polarization. However, the TE spectra are dominated by the multilayer eigenmodes which appear as a set of six modes almost parallel to each other. These are slab modes of the TiO_2/SiO_2 multilayer, but due to the presence of the periodic array can now leak outside. The coupling of these modes to the sphere array modes of the same symmetry will finally lead to hybridization minigaps when modes cross.

IV. CONCLUSIONS

We have investigated visible and infrared resonant absorbers and proposed different possibilities to achieve perfect absorption with metals and dielectrics. We offered a simple and efficient quantitative analysis of resonant absorption based on scattering theory, which can be also used for the design of simple subwavelength optical coatings demonstrated recently[46,47] or metamaterial perfect absorbers. Our results would be useful in the design of perfect absorbers using particle arrays in front of reflectors since particles of different shapes like nanorods, nanorings, etc., could be similarly optimized to achieve perfect light absorbers.

ACKNOWLEDGMENTS

E. Almpanis was supported by NCSR "Demokritos" through a postgraduate fellowship.

APPENDIX ABSORPTION OF A LOSSY RESONATOR IN FRONT OF A REFLECTOR

We follow the appendix of Gantzounis and Stefanou[48] and proceed further by considering dissipative losses. Our approach relies on general properties of the scattering matrix S implied from the causality condition.[37,49] For a lossless

structure comprising a planar total reflector, the S matrix is unitary and, since transmission vanishes, its eigenvalues are reduced to the appropriate reflection coefficients which have the form[48]

$$r(\omega) = e^{2i\phi}\frac{\omega - \omega_n - i\gamma_{rad}}{\omega - \omega_n + i\gamma_{rad}} \tag{A1}$$

about the resonance frequencies ω_n. The analytic continuation of these eigenvalues implies zeros in the upper complex plane at $\omega_n + i\gamma_{rad}$ and poles in the lower half at $\omega_n - i\gamma_{rad}$. From this form, it is easy to obtain the local density of photonic states in the vicinity of ω_n[48]

$$\Delta n(\omega) \approx \frac{1}{\pi}\frac{\gamma_{rad}}{(\omega - \omega_n)^2 + {\gamma_{rad}}^2}. \tag{A2}$$

The distance of a pole (zero) from the real axis is directly related to the half-width at half maximum of the resonance and γ_{rad} is the associated decay rate. If losses are introduced in the system, then the S matrix is no longer unitary and the poles and zeros of its eigenvalues are shifted down in the complex frequency plane by an additional amount $-i\gamma_{nr}$.[37] Therefore in the dissipative system, we have

$$r(\omega) = e^{2i\phi}\frac{\omega - \omega_n - i(\gamma_{rad} - \gamma_{nr})}{\omega - \omega_n + i(\gamma_{rad} + \gamma_{nr})}, \tag{A3}$$

where the phase ϕ becomes complex: $\phi = \theta + i\alpha$. In this case, since transmittance is zero, the absorbance in the vicinity of a resonance is given by

$$\mathcal{A} = 1 - |r(\omega)|^2 = 1 - e^{-4\alpha} + \frac{4e^{-4\alpha}\gamma_{rad}\gamma_{nr}}{(\omega - \omega_n)^2 + (\gamma_{rad} + \gamma_{nr})^2}. \tag{A4}$$

This equation includes losses away from the resonant frequency and is identical to Eq. (11) of Ref. 38 if $\alpha = 0$. Assuming that α is frequency independent within the resonance bandwidth, Eq. (A4) allows for the determination of γ_{rad}, γ_{nr}, and α by fitting the relevant absorption spectra. We note that γ_{rad} can also be extracted independently from the local density of states calculated for the corresponding lossless structure.

[1] E. F. Knott, J. F. Shaeffer, and M. T. Tuley, *Radar Cross Section*, 2nd ed. (Scitech Publication, Raleigh, 2006).
[2] N. Stefanou and A. Modinos, J. Phys. Condens. Matter **3**, 8149 (1991).
[3] M. G. Nielsen, A. Pors, O. Albrektsen, and S. I. Bozhevolnyi, Opt. Express **20**, 13311 (2012).
[4] H. Y. Zheng, X. R. Jin, J. W. Park, Y. H. Lu, J. Y. Rhee, W. H. Jang, and Y. P. Lee, Opt. Express **20**, 24002 (2012).
[5] P. Ding, E. Liang, G. Cai, W. Hu, C. Fan, and Q. Xue, J. Opt. **13**, 075005 (2011).
[6] Y. Cui, K. H. Fung, J. Xu, S. He, and N. X. Fang, Opt. Express **20**, 17552 (2012).
[7] X. Shen, T. J. Cui, J. Zhao, H. F. Ma, W. X. Jiang, and H. Li, Opt. Express **19**, 9401 (2011).
[8] A. Polyakov, S. Cabrini, S. Dhuey, B. Harteneck, P. J. Schuck, and H. A. Padmore, Appl. Phys. Lett. **98**, 203104 (2011).
[9] N. I. Landy, S. Sajuyigbe, J. J. Mock, D. R. Smith, and W. J. Padilla, Phys. Rev. Lett. **100**, 207402 (2008).
[10] J. Hao, J. Wang, X. Liu, W. J. Padilla, L. Zhou, and M. Qiu, Appl. Phys. Lett. **96**, 251104 (2010).
[11] H. Tao, N. I. Landy, C. M. Bingham, X. Zhang, R. D. Averitt, and W. J. Padilla, Opt. Express **16**, 7181 (2008).
[12] J. Hao, L. Zhou, and M. Qiu, Phys. Rev. B **83**, 165107 (2011).
[13] Z. Fang, Y.-R. Zhen, L. Fan, X. Zhu, and P. Nordlander, Phys. Rev. B **85**, 245401 (2012).
[14] C. Wu, Y. Avitzour, G. Shvets, M. A. Noginov, and N. I. Zheludev, Proc. SPIE **7029**, 70290W (2008).
[15] Y. Avitzour, Y. A. Urzhumov, and G. Shvets, Phys. Rev. B **79**, 045131 (2009).
[16] J. Zhang, J.-Y. Ou, K. F. MacDonald, and N. I. Zheludev, J. Opt. **14**, 114002 (2012).
[17] K. Aydin, V. E. Ferry, R. M. Briggs, and H. A. Atwater, Nat. Commun. **2**, 517 (2011).
[18] P. Bouchon, C. Koechlin, F. Pardo, R. Haïdar, and J.-L. Pelouard, Opt. Lett. **37**, 1038 (2012).
[19] H. Li, L. H. Yuan, B. Zhou, X. P. Shen, Q. Cheng, and T. J. Cui, J. Appl. Phys. **110**, 014909 (2011).
[20] D. Y. Shchegolkov, A. K. Azad, J. F. OHara, and E. I. Simakov, Phys. Rev. B **82**, 205117 (2010).
[21] C. Guclu, S. Campione, and F. Capolino, Phys. Rev. B **86**, 205130 (2012).
[22] C. Hägglund, S. P. Apell, and B. Kasemo, Nano Lett. **10**, 3135 (2010).
[23] H. A. Atwater and A. Polman, Nature Mater. **9**, 205 (2010).
[24] N. C. Lindquist, W. A. Luhman, S. H. Oh, and R. J. Holmes, Appl. Phys. Lett. **93**, 123308 (2008).
[25] J. N. Munday and H. A. Atwater, Nano Lett. **11**, 2195 (2011).
[26] N. Liu, M. Mesch, T. Weiss, M. Hentschel, and H. Giessen, Nano Lett. **10**, 2342 (2010).
[27] J. J. Talghader, A. S. Gawarikar, and R. P. Shea, Light: Sci. Appl. **1**, e24 (2012).
[28] Z. Ruan and S. Fan, Phys. Rev. Lett. **105**, 013901 (2010).
[29] B. S. Lukyanchuk, A. E. Miroshnichenko, M. I. Tribelsky, Y. S. Kivshar, and A. R. Khokhlov, New J. Phys. **14**, 093022 (2012).
[30] M. I. Tribelsky, Europhys. Lett. **94**, 14004 (2011).
[31] H. Noh, Y. Chong, A. D. Stone, and H. Cao, Phys. Rev. Lett. **108**, 186805 (2012).
[32] C. Tserkezis, G. Gantzounis, and N. Stefanou, J. Phys. Condens. Matter **20**, 075232 (2008).
[33] T. Søndergaard, S. M. Novikov, T. Holmgaard, R. L. Eriksen, J. Beermann, Z. Han, K. Pedersen, and S. I. Bozhevolnyi, Nat. Commun. **3**, 969 (2012).
[34] P. Spinelli, M. A. Verschuuren, and A. Polman, Nat. Commun. **3**, 692 (2012).
[35] A. Raman, Z. Yu, and S. Fan, Opt. Express **19**, 19015 (2011).
[36] M. Albooyeh and C. R. Simovski, Opt. Express **20**, 21888 (2012).
[37] Y. D. Chong, L. Ge, H. Cao, and A. D. Stone, Phys. Rev. Lett. **105**, 053901 (2010).
[38] J. Yoon, K. H. Seol, S. H. Song, and R. Magnusson, Opt. Express **18**, 25702 (2010).
[39] N. Stefanou, V. Yannopapas, and A. Modinos, Comput. Phys. Commun. **113**, 49 (1998).
[40] N. Stefanou, V. Yannopapas, and A. Modinos, Comput. Phys. Commun. **132**, 189 (2000).
[41] N. Papanikolaou, Phys. Rev. B **75**, 235426 (2007).
[42] B. Johnson and R. W. Christy, Phys. Rev. B **6**, 4370 (1972).
[43] D. E. Aspnes, *in Properties of Silicon, EMIS Data Reviews* (Inspec IEE, London, 1988).
[44] M. López-García, J. F. Galisteo-López, C. López, and A. García-Martín, Phys. Rev. B **85**, 235145 (2012).
[45] J. Grandidier, D. M. Callahan, J. N. Munday, and H. A. Atwater, Adv. Mater. **23**, 1272 (2011).
[46] M. A. Kats, R. Blanchard, P. Genevet, and F. Capasso, Nature Mater. **12**, 20 (2013).
[47] M. A. Kats, D. Sharma, J. Lin, P. Genevet, R. Blanchard, Z. Yang, M. M. Qazilbash, D. N. Basov, S. Ramanathan, and F. Capasso, Appl. Phys. Lett. **101**, 221101 (2012).
[48] G. Gantzounis and N. Stefanou, Phys. Rev. B **72**, 075107 (2005).
[49] N. G. van Kampen, Phys. Rev. **89**, 1072 (1953).